

Galaxy Colour, Morphology, and Environment in the Sloan Digital Sky Survey

N. M. Ball,^{1,2*} J. Loveday³ and R. J. Brunner^{1,2}

¹Department of Astronomy, MC-221, University of Illinois, 1002 West Green Street, Urbana, IL 61801, USA

²National Center for Supercomputing Applications, MC-476, University of Illinois, 605 East Springfield Avenue, Champaign, IL 61820, USA

³Astronomy Centre, University of Sussex, Falmer, Brighton, BN1 9QJ, UK

Accepted xxxx Received xxxx

ABSTRACT

We use the Fourth Data Release of the Sloan Digital Sky Survey to investigate the relation between galaxy colour and environmental density for a sample of 79,553 galaxies at $z \lesssim 0.1$ and compare it to that between morphology and density for a sample of 13,655 galaxies with Hubble types assigned by an artificial neural network. As found by previous authors, the rest frame $u - r$ is well described by a sum of two Gaussians, forming a bimodal distribution. In contrast, the Hubble type morphology is not well described by such a sum. This indicates that either (1) there are more than two significant populations in morphology, for example elliptical, S0, and spiral; (2) that there are physical processes not seen in colour space, or (3) that the morphological measures, particularly the different subtypes of spirals Sa–Sd, are intrinsically ‘fuzzy’ when related to environmental density. It is not likely an artefact of using a neural network as these have been shown to perform very similarly to human classifiers. On removing the density relation due to morphology, we find a residual relation due to colour, however on removing the colour-density relation there is no evidence for a residual relation due to morphology.

Key words: cosmology: observations – methods: data analysis – methods: statistical – galaxies: fundamental parameters – galaxies: statistics

1 INTRODUCTION

The connection between the morphology of a galaxy and the density of its environment, measured in a variety of ways, is an important clue to the physics of galaxy formation, and forms a readily observable quantity that can be compared with simulations. Numerous physical processes affect the evolution of a galaxy as a function of its density environment. The debate is ongoing as to which of these are intrinsic to the galaxies at formation and which are the result of later evolution.

The relative importance of different processes depends on the density of the environment. For example, in clusters infalling galaxies are subject to ram-pressure stripping and galaxy harassment. In groups, mergers, interactions and strangulation are more important. It is thought that ellipticals formed their stars early, exhausting their gas supply and are now passively evolving in dense environments, whereas spirals formed their stars more slowly, continuing to the present day and becoming subject to the physical processes described on infall into denser environments as the structure evolved. More detailed recent reviews of the subject include (Boselli & Gavazzi 2006; Avila-Reese 2006; Hogg 2005).

However, the morphology of the galaxies is affected in ways

not necessarily correlated with the effect on spectral properties or colour. One can therefore investigate the morphology-density and colour-density relations and subtract the two to see if a residual relation remains. If so, then there is an intrinsic effect of density that is not a result of a more fundamental process which causes the other relation.

A particular example of this is the hypothesis that the properties of galaxies within a dark matter halo depend only on the mass of the halo (e.g. Cooray & Sheth 2002). This can be tested both for colour and for morphology, although here we do not specifically relate our results to haloes. Recent results such as Blanton et al. (2006) and Abbas & Sheth (2006) support this assumption.

An example of a physical process causing a distinct change in morphology is that of S0 galaxies. Christlein & Zabludoff (2004) find that they must have formed from bulge enhancement and not disc fading. Boselli & Gavazzi (2006) find that S0s are formed through gravitational interaction rather than spiral interaction with the intergalactic medium.

Here, we use the Fourth Data Release (DR4, Adelman-McCarthy et al. 2006) of the Sloan Digital Sky Survey (SDSS, York et al. 2000) to investigate these relations. The colour-density relation was previously investigated by Balogh et al. (2004, hereafter B04). They found a pronounced bimodal distribution well-fit by a sum of two Gaussians. At fixed luminosity, the mean colours of the

* E-mail: nball@astro.uiuc.edu

two distributions were approximately independent of environment, but the red fraction strongly increased with density. The density measure used was the projected distance to the fifth nearest neighbour in a redshift slice of width 1000 km s^{-1} . Here we use the same density measure and compare the distributions in colour to those in morphology. We also divide the relations by luminosity, as done in B04.

The main measure of morphology used is the Hubble type assigned by an artificial neural network (ANN, Ball et al. 2004). This assigns T types 0–6, corresponding to E, S0, Sa, Sb, Sc, Sd and Im, to a limiting magnitude of $r < 15.9$. We supplement this with a sample to $r < 17.77$ for which the Petrosian inverse concentration index (CI_{inv}) and Sérsic index n are measured. These provide a simpler measure of morphology but for a larger sample, corresponding to the SDSS Main Galaxy Sample (Strauss et al. 2002).

Previous work in the SDSS on the morphology-density relation includes Goto et al. (2003), in which they use the concentration index and the texture parameter of Yamauchi et al. (2005) to study galaxies in the SDSS Early Data Release (EDR, Stoughton et al. 2002). Their results are described further in §3.3 below.

Throughout, the standard spatial geometry is assumed, with Euclidean space, $\Omega_{\text{matter}} = 0.3$, $\Omega_{\Lambda} = 0.7$ and dimensionless Hubble constant $h = 1$, where $h = H_0/100 \text{ km s}^{-1} \text{ Mpc}^{-1}$.

2 DATA

The SDSS is a project to map π steradians of the northern galactic cap in five bands (u , g , r , i and z) from $3,500$ – $8,900 \text{ \AA}$. This will provide photometry for of order 5×10^7 galaxies. A multifibre spectrograph will provide redshifts and spectra for approximately 10^6 of these. A technical summary of the survey is given in York et al. (2000). The telescope is described in Gunn et al. (2006). The imaging camera is described in Gunn et al. (1998). The photometric system and calibration are described in Fukugita et al. (1996), Hogg et al. (2001), Smith et al. (2002), Ivezić et al. (2004) and Tucker et al. (2006). The astrometric calibration is in Pier et al. (2003) and the data pipelines are in Lupton et al. (2001), Lupton (2006) for the deblender, Frieman et al. and Schlegel et al. (in preparation).

The targeting pipeline (Strauss et al. 2002) chooses targets for spectroscopy from the imaging. A tiling algorithm (Blanton et al. 2003) then assigns the spectroscopic fibres to the targets, the main source of incompleteness being the minimum distance of 55 arcsec between the fibres. This causes about 6% of galaxies to be missed; those that are will be biased towards regions with a high surface density of galaxies. The algorithm gives a more uniform completeness on the sky than a uniform tiling by taking into account large scale structure, but the effect is still present. The other main source of incompleteness is galaxies blended with saturated stars, which is a 1% level effect. The overall spectroscopic completeness is therefore estimated to be over 90% (Strauss et al. 2002).

The SDSS galaxies with spectra consist of a ‘Main’, flux-limited sample, with a median redshift of 0.104 (Strauss et al. 2002), a luminous red galaxy sample (LRG), approximately volume-limited to $z \approx 0.4$ (Eisenstein et al. 2001) and a quasar sample (Richards et al. 2002). The limiting magnitude for the Main spectra is $r < 17.77$, which is substantially brighter than that for the imaging so the redshift completeness is almost 100%. A typical signal-to-noise value is > 4 per pixel and the spectral resolution is 1800. The redshifts have an RMS accuracy of $\pm 30 \text{ km s}^{-1}$.

We use galaxies from the Main Galaxy Sample. The data are extracted from the New York Value-Added Galaxy Catalogue

(VAGC, Blanton et al. 2005). They are masked, extinction- and K-corrected in the same way as the datasets in Ball et al. (2006, hereafter B06). There is no correction for evolution, but as the redshifts are limited to $z \lesssim 0.1$ its effects are not large. Similarly, there is no correction for dust, but this is mitigated by the requirement that the galaxy axis ratio be less than that of an E7 galaxy, as described in B06.

2.1 Galaxy Environment

The masking of the dataset as in B06 leaves a sample of 489,123 galaxies. These are matched to the galaxies in the Pittsburgh-CMU Value Added Catalogue (VAC, http://nvogre.phyast.pitt.edu/dr4_value_added). The matches were carried out using the unique identification, both in object and date of observation, provided by the spectroscopic plate, mjd and fibre values for each object. The matches were made in order to utilize their measures of the distance from each galaxy to the nearest survey edge, which use a sophisticated algorithm taking into account the full survey mask. Galaxies measured by the VAC as being nearer to a survey edge than their Nth nearest neighbour are excluded to prevent the densities being biased downward near the survey edge or at the higher redshifts in the sample.

We do, however, calculate our own environmental densities, as the VAC sample is restricted to the range $0.053 < z < 0.093$ to gain an improved measure of the star formation rate, which is not considered here. We follow the method of B04: the density is given by $\Sigma_N = N/\pi d_N^2$ where d_N is the distance to the Nth nearest neighbour within $\pm 1000 \text{ km s}^{-1}$ in redshift. This is used to minimize contamination from interlopers. Here the value of N used is 5, following B04 who choose this value to approximate Dressler (1980) which uses $N = 10$ before correction for superimposed galaxies. We bin the sample in steps of 0.5 over the range $-1.5 < \log \Sigma_5 < 1.5$, a factor of 1,000 in density.

We set a limiting absolute magnitude for galaxies to be counted as neighbours of $M_r - 5\log h < -19.5$, corresponding to one magnitude fainter than the value of M^* found for the overall Schechter fit to the galaxy luminosity function of B06. The corresponding limiting redshift, at which a galaxy of this magnitude has an apparent magnitude $r = 17.77$ is $z < 0.0889$. This gives a sample volume-limited to a distance comparable to the $z < 0.08$ of B04. We also require $z > 0.001$ to exclude very local objects. We measure densities for galaxies in the range M_{-2}^{*+3} , i.e. $-22.5 < M_r - 5\log h < -17.5$, binning in steps of one magnitude. This again is similar to the range of $-22.23 < M_r - 5\log h < -17.23$ of B04.

2.2 Galaxy Colour and Morphology

We use $u - r$ colour following B04 and Baldry et al. (2004b), who find that the galaxy population is well described as the sum of two Gaussians in $u - r$, with an optimal colour separator of 2.22 (Strateva et al. 2001). We use the model colours from the same dataset as B06, extinction- and K-corrected, as in that paper, to a rest-frame band-shift of $z = 0.1$. The model colours are derived from the SDSS model magnitudes. For each galaxy these are derived from the best fitting of a de Vaucouleurs (de Vaucouleurs 1948) or exponential profile (Freeman 1970).

The ANN morphologies used were also the same as those in B06, assigned as in Ball et al. (2004) and updated as described in B06. The types assigned correspond to the Hubble types E=0,

$S0=1$, $Sa=2$, $Sb=3$, $Sc=4$, $Sd=5$ and $Im=6$. As described in B06, there is bias away from the ends of the scale, particularly for late types. This is probably due to the dominant contribution of the concentration index in the training set, which shows a similar bias, and the relative lack of types of Sd or later in the training set in part due to the r band selection of the SDSS instead of the more commonly used bluer bands. Hence the latest types assigned have $T_{\text{ANN}} \sim 4.5$. We bin the ANN morphologies in five bins from -0.5 – 4.5 . The colours are also binned in five bins. Unlike the other measures presented, the limiting magnitude for the ANN morphologies is $r < 15.9$, as this was the faintest level to which the visually assigned training set was generated. Of the galaxies studied here, 13,655 have a value for T_{ANN} and a valid density. Combined with the absolute magnitude limit of $M_r - 5\log h < -17.5$, these limits ensure that there is no extrapolation from the ANN training set in apparent or absolute magnitude.

We supplement the sample of ANN morphologies with the inverse concentration index, CI_{inv} , and the Sérsic index n . These provide a simpler measure of morphology but are measured for the full $r < 17.77$ sample. The CI_{inv} is given by R_{50}/R_{90} where R_N is the $N\%$ light Petrosian radius (see, e.g. Stoughton et al. 2002). The inverse is used because it has the range 0–1. The Sérsic index is the exponent in the formula for a generalized galaxy light profile given by Sérsic (1968), or more recently in e.g. Graham & Driver (2005). Because n is an exponent, and the bimodality shows more clearly when it is done so, n is binned logarithmically, as with the density. As with the colours, these are binned appropriately, giving bins of $0.23 < CI_{\text{inv}} < 0.58$ in steps of 0.07 and $-0.25 < \log n < 0.75$ in steps of 0.2. Parameters other than colours are measured in the r band, since this band is used to define the aperture through which Petrosian flux is measured for all five bands.

For each set of measurements, the galaxies are required to have values within the ranges of the bins of all quantities that are binned, i.e. density, luminosity, and one or both of colour and morphology. This ensures that each related figure is showing the same galaxies. The resulting samples consist of 79,553 galaxies for $u-r$, 13,655 for T_{ANN} , 79,606 for CI_{inv} and 75,861 for Sérsic index. For the residuals in $u-r$ and T_{ANN} , requiring both colour and morphology to be within the bin ranges reduces the sample size to 13,638.

2.3 Data Fitting

The data points for the histograms of $u-r$ and T_{ANN} for bins of $\log \Sigma_5$ and M_r are fitted using a simplex search algorithm over the ranges $0.5 < u-r < 4.0$ and $0 < T_{\text{ANN}} < 4.5$. The number of galaxies outside these ranges is small, being less than 1% of the total. The fits involve six parameters and are given by

$$A N(\bar{x}_1, \sigma_1) + B N(\bar{x}_2, \sigma_2), \quad (1)$$

where the $N(\bar{x}, \sigma)$ are Gaussians with mean \bar{x} and standard deviation σ and A and B are scalars. Whereas B04 constrain the σ values of the Gaussians to be functions of M_r only, here we do not apply any restrictions on the parameters of the two Gaussians in one plot relative to any others. The fit do not utilize the extreme ends of the distributions, where there are very few galaxies.

Again following B04, the 1σ error bars for each bin are given by $\sqrt{N_{\text{bin}} + 2}$ where N_{bin} is the number of galaxies in that bin. This is an approximation of the Poisson error for small number statistics.

3 RESULTS

3.1 Colour and Hubble Type Morphology

Fig. 1 shows the rest-frame $u-r$ colour distribution in bins of $\log \Sigma_5$. The distribution is clearly bimodal and is well fit by two Gaussians, confirming the idea of two separate populations described by numerous authors (e.g. Baldry et al. 2004b). As expected, the fraction of blue galaxies decreases with density. The position of the blue peak moves redwards from $u-r \approx 1.5$ to $u-r \approx 2.25$ and that of the red peak stays approximately constant, with just a slight reddening from $u-r \approx 2.5$ to $u-r \approx 2.75$. Unlike the peaks, the position of the minimum between the two distributions stays constant, although in the two highest density bins the exact position of the minimum is unclear. B04 find that at fixed luminosity the position of the colour peaks does not change with density, but that there is a weak trend for colours to become redder at high densities, which agrees qualitatively with the results here.

Fig. 2 shows the restframe $u-r$ colour distribution in bins of absolute magnitude M_r . A similar trend is seen with the red peak moving slightly bluewards and dropping in fraction with decreasing luminosity and the blue peak becoming bluer. Bright galaxies at $M_r - 5\log h < -21.5$ are relatively rare as are faint galaxies due to the $r < 17.77$ limit for spectra.

Fig. 3 shows the T_{ANN} distribution in bins of $\log \Sigma_5$, which is the morphology-density relation. A sum of two Gaussians is now a much worse fit to the data, with a clear excess of galaxies at $T_{\text{ANN}} \sim 1$ at densities $\log \Sigma_5 \gtrsim -0.3$. The expected dominance of early types at high density is seen and the peak narrows with density. The late type peak becomes lower and earlier, in a similar manner to the reddening of the blue peak in $u-r$. The lack of (or less clear) division into a bimodal population suggests that if galaxies really are divided into just two dominant populations then either (1) the morphology is insensitive to it, spreading between the two; (2) that morphology is more sensitive to transitional states between the two, such as $S0$ galaxies, than colour, or (3) the morphology is an intrinsically ‘fuzzy’ measure, resulting in a inevitable spread across types. If (2) is correct, such a transitional state must then be rare and/or brief in colour space for the clear division in colour to be seen as $S0$ galaxies are not rare. That the transitional population is clearest at higher densities is also consistent with it being $S0$ s. (3) is less likely for the overall population, i.e. one can split $E/S0$ from spiral, but the excess over Gaussian at $T_{\text{ANN}} \sim 1$ and at very late types supports the ‘fuzzy’ nature of the morphological classification. The spread is not likely to be an artefact of typing via neural network, as these were shown (e.g. Storrie-Lombardi et al. 1992; Naim et al. 1995; Ball et al. 2004) to perform with an RMS spread between true type and assigned type no different to that of human classifiers.

Fig. 4 shows the T_{ANN} distribution in bins of M_r . The change from early to late type dominance from bright to faint is clear and the other trends described above for morphology-density are also seen here.

Fig. 5 shows $u-r$ subdivided by both Σ_5 and M_r , i.e. dividing Fig. 1 by luminosity. This is an update of fig. 1 of B04, using DR4 rather than DR1 and with the differences described in §2 above. As mentioned, B04 find that at fixed luminosity the mean colours of the two distributions are nearly independent of density, but that the fraction of red galaxies rises sharply at all luminosities. As expected, our plot shows the same trends. Fig. 6 shows the same but for T_{ANN} . As above, the pattern is less obviously bimodal than for $u-r$.

Figs. 7–9 show some of the trends in Figs. 5 and 6 more

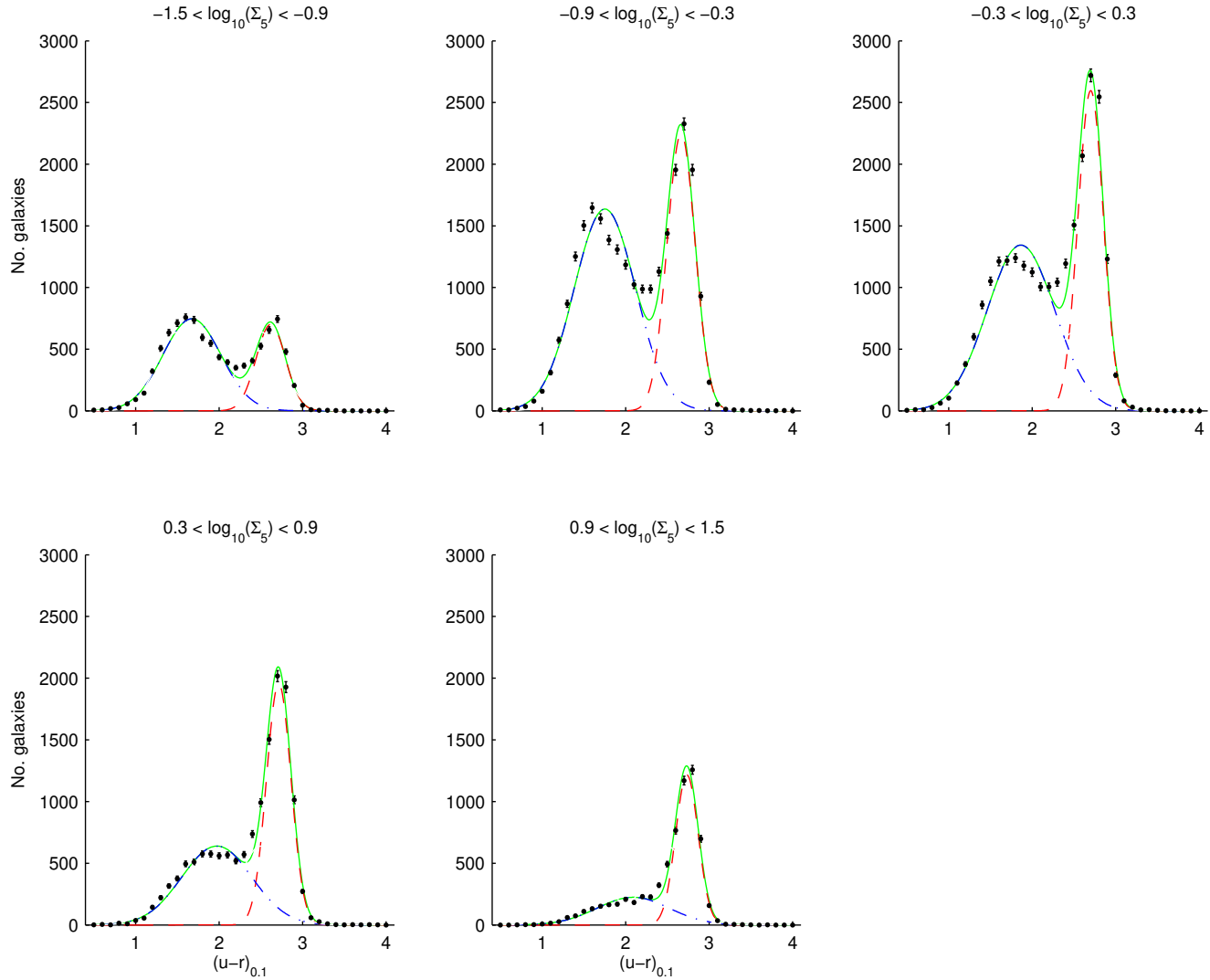


Figure 1. Numbers of galaxies in rest-frame $u - r$ versus Σ_5 surface density of galaxies. The points are the number of galaxies in each bin; the error bars are given by $\sqrt{N_{\text{bin}} + 2}$ where N_{bin} is the number of galaxies in that bin; the solid line is the best fit of the sum of two Gaussians using a simplex search; the dot-dash and dashed lines are the individual Gaussians. The vertical axes in each panel are given equal heights for clarity.

clearly. The $\pm 1\sigma$ error bars are calculated by finding the point at which the χ^2 for the fit increases by 1 around the minimum for each parameter in turn. The shape of the χ^2 is assumed to be parabolic, which is a good approximation, although it assumes that the χ^2 is minimized for the other parameters whilst the one under study is being varied. However, these approximations will tend to overestimate the errors, so it is good as a conservative estimate.

The left hand panel of Fig. 7 shows the fraction of red galaxies for M_r versus Σ_5 for $u - r$. The fraction is given by the ratio of the areas under the two Gaussians, which is given by $A/(A + B)$ assuming that approximately the whole area under each Gaussian is populated by galaxies (the normalised areas are 1). This is seen to be true in Figs. 1–6. The fraction, as expected, is seen to rise with density. The fraction also rises in a similar way over all luminosities, although the brightest galaxies at $-22.5 < M_r - 5\log h < -21.5$ are rather noisy. The trends are similar to those in the left hand panel of fig. 2 in B04.

The left hand two plots of Fig. 8 show the mean colours \bar{x}_1 and \bar{x}_2 in a similar way for the two Gaussians. The mean colour for

the red galaxies is approximately independent of density (as seen in Fig. 1), with just a slight trend for redder colours at higher densities. The blue galaxies show a more distinct reddening towards the highest densities. This is similar to fig. 3 of B04.

The left hand two plots of Fig. 9 show the dispersions σ_1 and σ_2 . For red galaxies the dispersions are low and decline at the highest density, suggesting a tendency towards the same colour with density, whilst those for the blue galaxies are higher, increasing at the highest density. The dispersions for red galaxies also show a clear decrease with increasing luminosity.

The right hand halves of Figs. 7–9 show the same as the left but for T_{ANN} . In Fig. 7, the early type fraction shows some increase with density in a similar way to the red fraction, whereas the late type fractions are noisy.

In Fig. 8 the mean type for the early type galaxies is seen to be approximately independent of density at fixed luminosity in the same way that colour was for the red galaxies. This hints that the same population is being seen, which is consistent with a distinct bright, concentrated, early spectral type, red population. The late

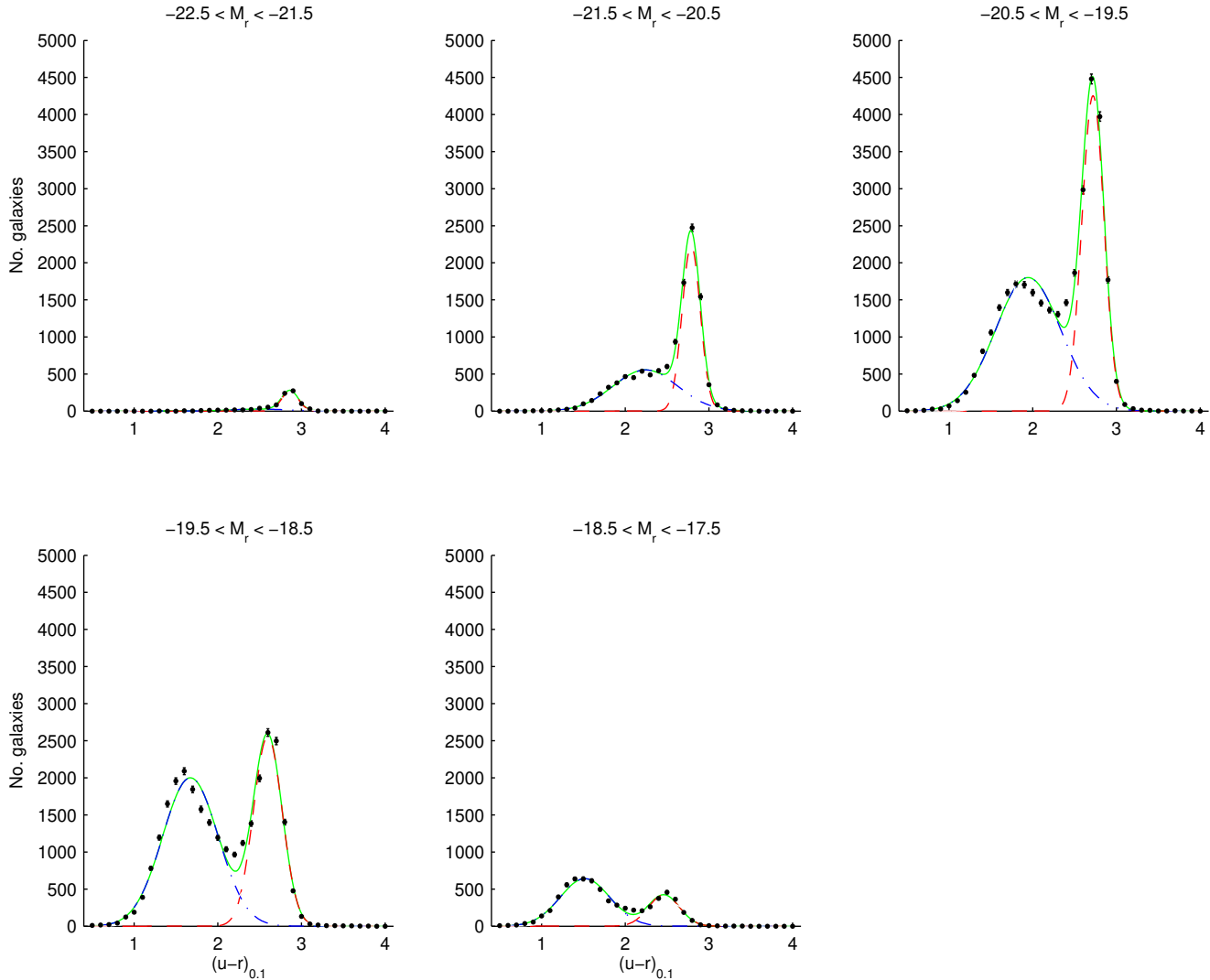


Figure 2. As Fig. 1 but subdivided by absolute magnitude.

types become earlier at high density in the manner of the blue galaxies in the left hand two plots. The similarity of the patterns seen suggests that in terms of the effect of environmental density, colour is closely correlated with morphology, but there could be a residual relation.

Fig. 9 shows that the dispersions are rather noisy for the morphological types and do not show any obvious change with density, justifying the constraint for them not to vary with $u-r$ in B04 (who also find little change if they do allow the dispersions to vary).

The residual relations are calculated by binning the galaxies into a 2-dimensional grid of colour and morphology, using the same histograms bins as in Figs. 1–6. The mean density μ_{ij} in each bin is calculated, along with the marginal averages as a function of colour bin (μ_i^c) and of morphology bin (μ_j^m), using the densities for the individual galaxies in each so that the bins are correctly weighted. In order to factor out the colour-dependence of density, one divides each mean density μ_{ij} by the appropriate marginal average μ_i^c . A re-calculation of the marginal dependence of density on colour would then give all ones, whereas a re-calculation of the marginal dependence on morphology will yield the residual morphology-dependence of density after that due to colour has been removed.

By instead dividing out the morphology-dependence in an equivalent way, the residual colour dependence may be calculated. The errors on each point are the 1σ dispersion of the values of the bins which are averaged to give that point.

The residual relations are plotted in Figs. 10 and 11. Fig. 10 shows the morphology-density relation after the removal of the change in density due to the change in colour with morphology. The residual relation is consistent with a value of one, i.e. no residual relation. This means that there is no evidence for a change in morphology that is not correlated with a change in colour. The spread and hence size of the error bars may be intrinsic to the Hubble type measure of morphology in the context of environment.

In contrast, Fig. 11 shows that there is a definite trend in density with colour when morphology is removed. This is consistent with numerous earlier studies (e.g. Blanton et al. 2005) in which the best predictor of environmental density was the colour. As expected, the density increases for redder galaxies. The error bars are still relatively large, reflecting the less certain nature of Σ_5 compared to colour.

In most of the plots in Figs. 1–6, the reduced χ^2 values, expected to be around 1 or less, of the double Gaussian fit are large.

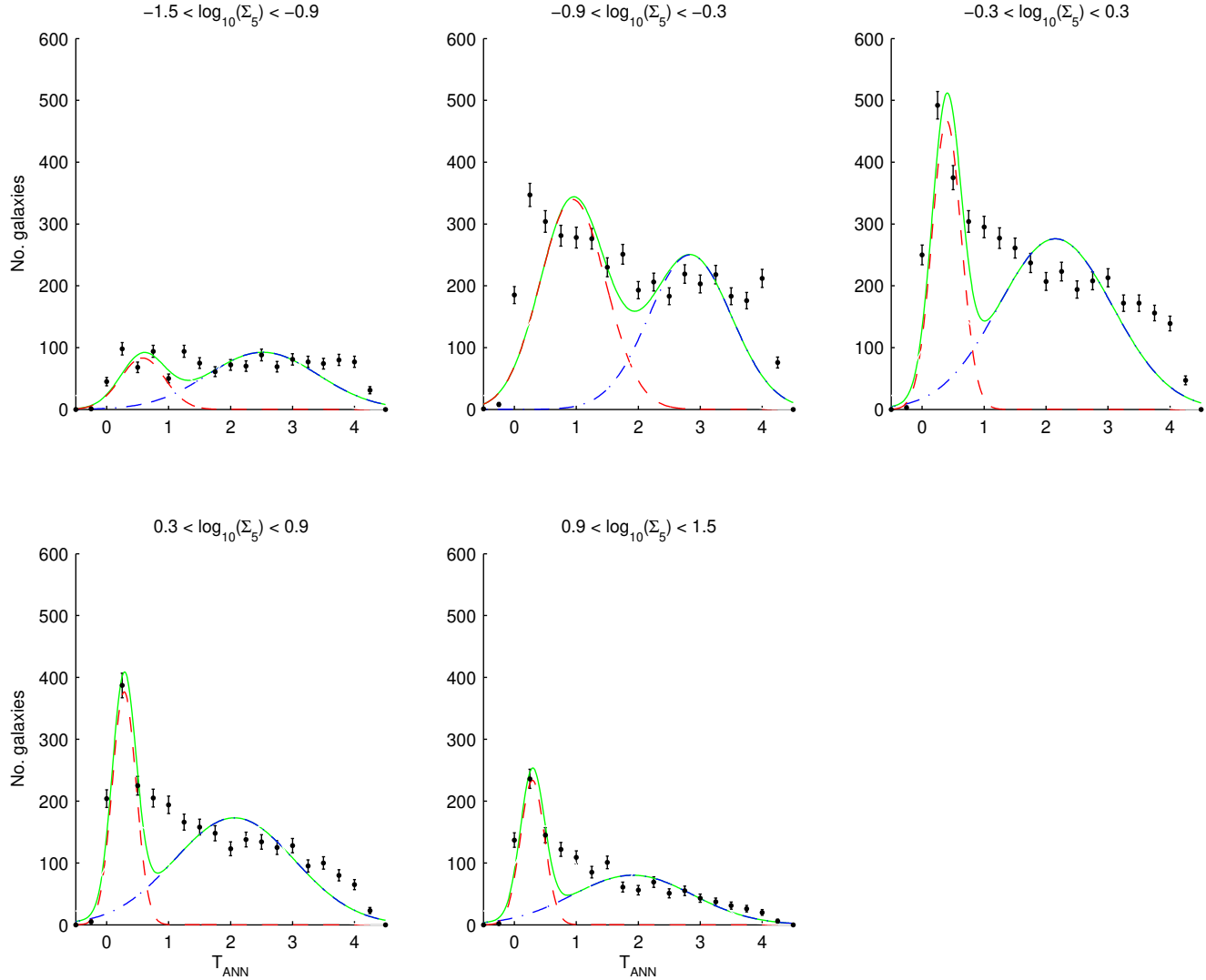


Figure 3. As Fig. 1 but for T_{ANN} subdivided by Σ_5 .

This was also seen in the χ^2 for fitting the bivariate LF in B06. As with those results, this is probably due to the small size of the error bars resulting from the large number of galaxies in the sample, indicating that the fitting function used is only an approximation to the data. What is clear is that the data is better fitted by two Gaussians than, say, one.

3.2 Concentration and Sérsic Index

Similar plots to Figs. 1–11 were also generated for the inverse concentration index CI_{inv} and Sérsic index n in place of T_{ANN} . The equivalent plots to Fig. 3 are shown in Figs. 12 and 14, and to Fig. 4 in Figs. 13 and 15. These distributions have not been fitted with double Gaussians.

The concentration index shows a more clearly bimodal distribution than the T type, although it becomes unimodal at very low and very high densities, with peaks at $CI_{\text{inv}} \sim 0.4$ and $CI_{\text{inv}} \sim 0.35$. Similar peaks are seen at $CI_{\text{inv}} \sim 0.3$ and $CI_{\text{inv}} \sim 0.4$ for high and low M_r . The values of CI_{inv} corresponding to the exponential spiral disc profile and the de Vaucouleurs elliptical galaxy

profile are 0.43 and 0.3 respectively, which match these peaks well, with perhaps some contamination.

The Sérsic index shows a bimodal distribution at all densities and all but the highest and lowest luminosities. The indices $n = 4$ ($\log n = 0.60$) and $n = 1$ ($\log n = 0$) correspond to de Vaucouleurs and exponential profiles. The peaks in the distribution are close to these values, but slightly nearer the overall mean, in a similar manner to CI_{inv} .

The bimodality seen suggests that either these are cleaner measures of morphology, or that the T type is sensitive to processes not seen here.

As with T_{ANN} , there are no obvious residual relations due to these measures of morphology when the relation due to colour is removed. Similar trends with colour to those seen for T_{ANN} , i.e. increasing residual density with redder galaxies, are seen when the morphology is removed. Thus the CI_{inv} and Sérsic indices are also not predictive of environment beyond their correlation to colour.

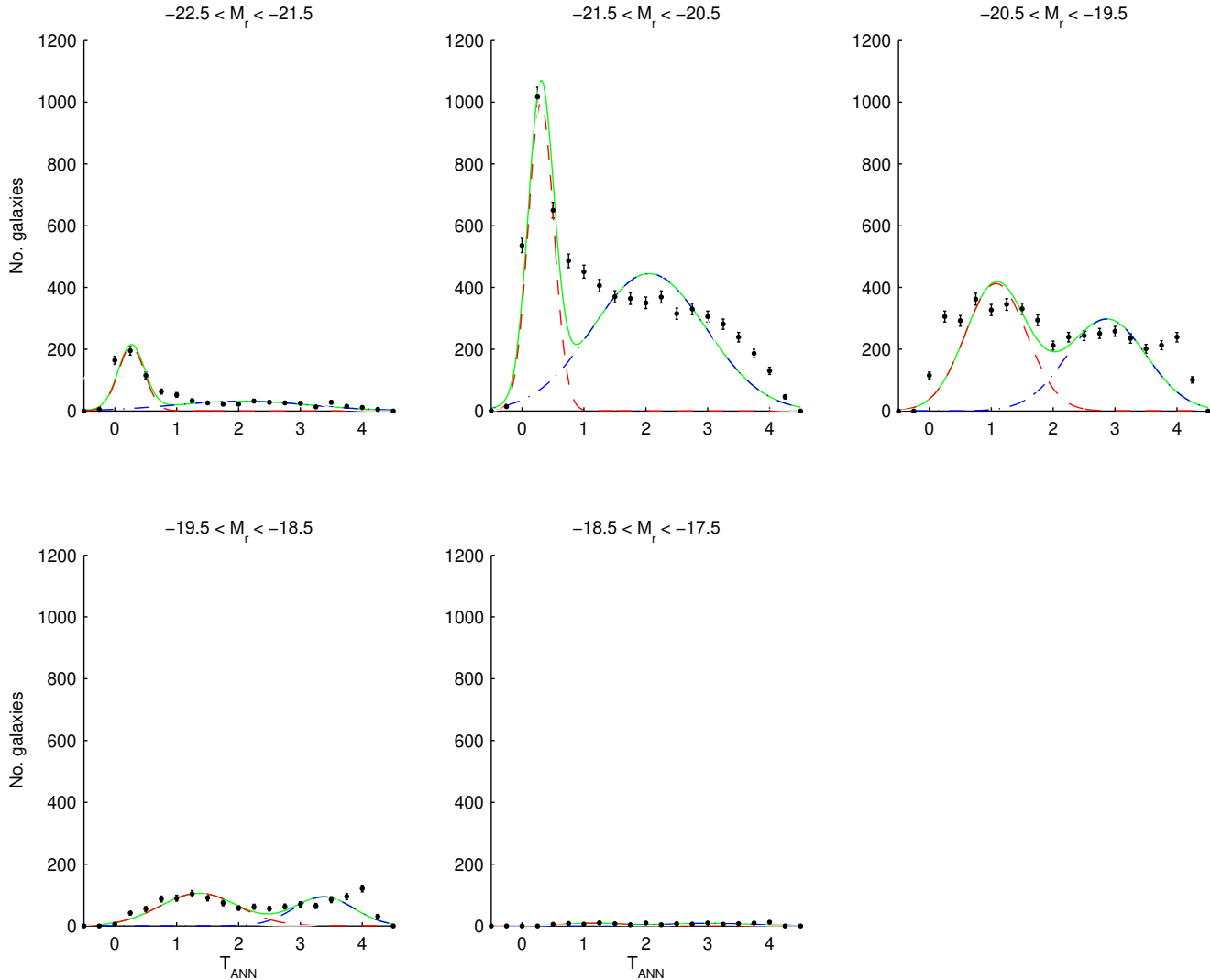


Figure 4. As Fig. 1 but for T_{ANN} subdivided by M_r .

3.3 Comparison to Previous Work

B04 presented the colour-density relation for the EDR, which has been compared to our results above.

Goto et al. (2003) present the morphology-density relation for the SDSS EDR. They assign morphology using the inverse concentration index, as used here, and a preliminary version of the texture parameter described by Yamauchi et al. (2005). The latter is corrected for elliptical isophotes and gives an improved correlation to visual morphology. The galaxies are divided into early, intermediate, early disc and late disc. The sample is volume-limited to $M_r - 5\log h < -19.9$ in the redshift range $0.05 < z < 1$ and contains 7,938 galaxies. This compares to our values of $M_r - 5\log h < -19.5$, $0.001 < z < 0.0889$ and 13,655 galaxies. The same $\Omega_{\text{matter}} = 0.3$, $\Omega_{\Lambda} = 0.7$ Euclidean cosmology is used. Their density estimator is three dimensional.

They find the expected trend of increasing early type fraction with increasing density, and also two characteristic scales, giving three density regimes. In the lowest density regime, the relation is less noticeable. In the intermediate density regime, intermediate type galaxies increase with density and spirals decrease. In the

densest regime, the intermediate types decrease and the early types increase. Thus the morphology is little affected in the low density regime, then subject to a mechanism which inhibits star formation and turns spirals into intermediate types in the intermediate density regime, then a third process decreases these types and increases early types in the dense regime.

Our work is consistent with this, with the bridge between the two bimodal populations resembling the intermediate types described here. It is difficult to compare quantitatively, however, as the density measures are different.

4 DISCUSSION

The question here is to what extent do the colour and T type morphology and in a broader sense other galaxy measures relate to the actual physics which is taking place. Does the morphology reveal anything that the colours do not? The results presented here enable this to be addressed by presenting a large sample of galaxy colours and morphologies within the same framework. The properties are also two of the parameters for which bivariate luminosity functions

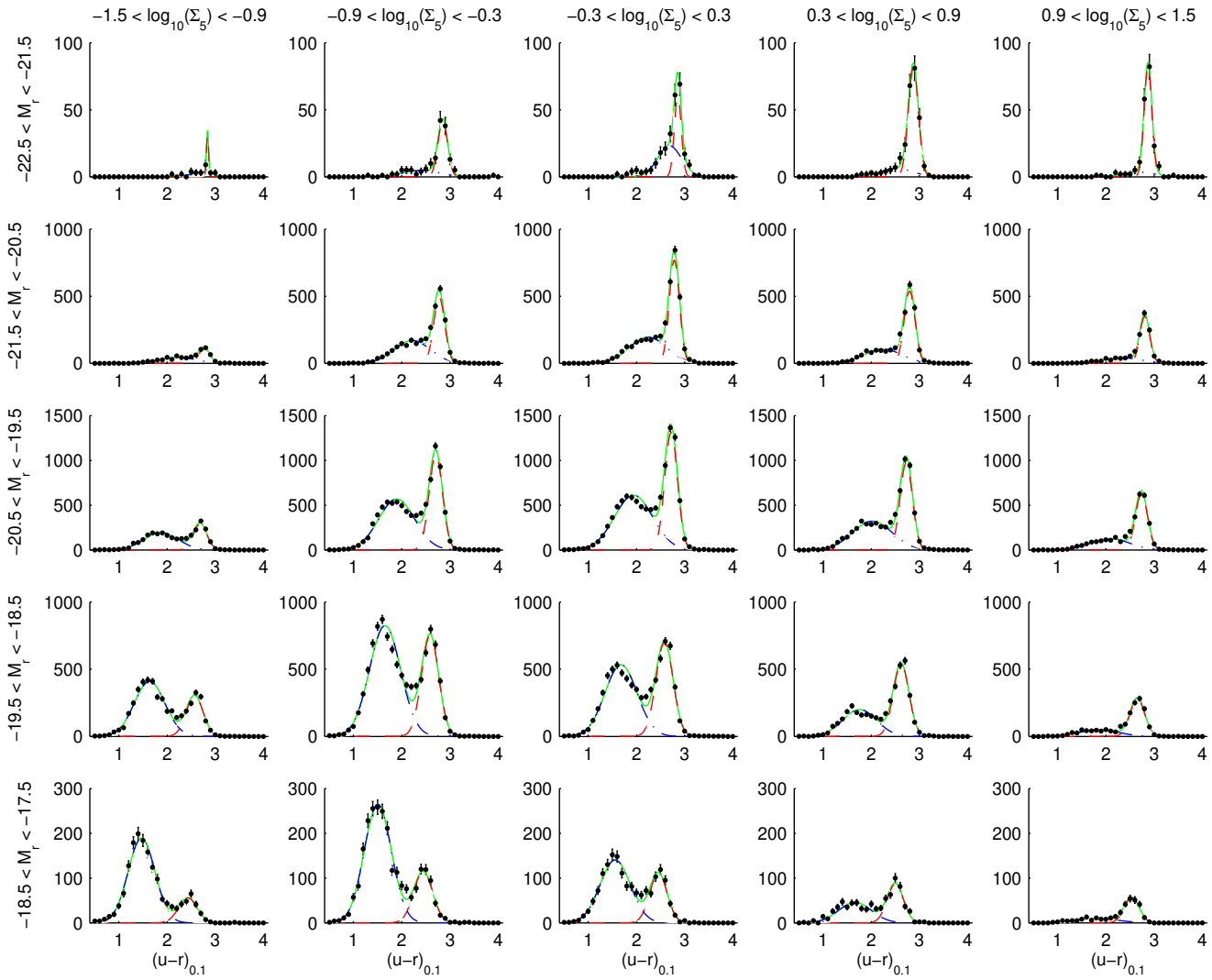


Figure 5. Numbers of galaxies for $u - r$ subdivided by Σ_5 and M_r . This reproduces the plot of Balogh et al. (2004) but for DR4 as opposed to DR1. The trends seen are very similar, as expected as DR4 is a superset of DR1.

(for a similar but not identical dataset) are plotted in B06 (their figs. 2 and 6).

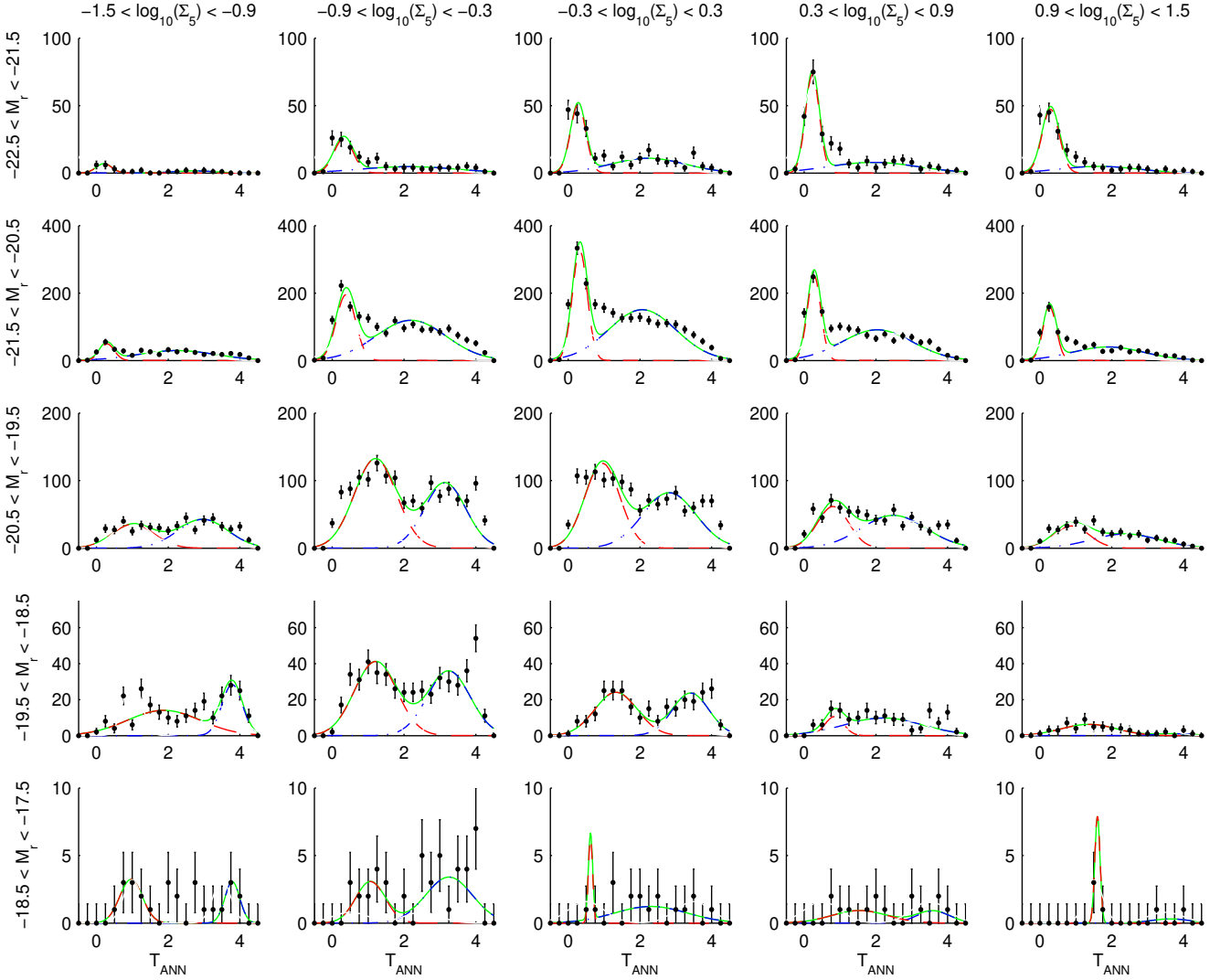
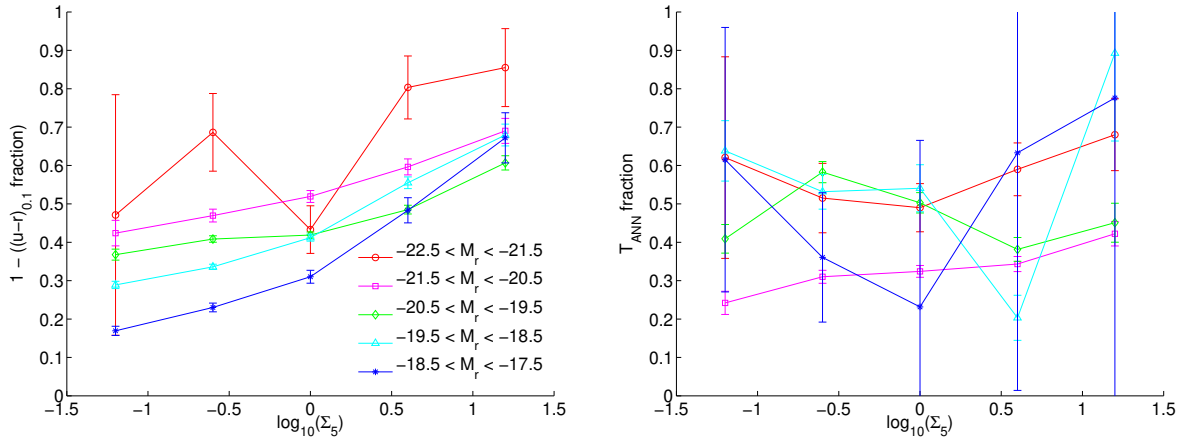
Considering the number of galaxies, the variety of their properties and environments and the quality of the SDSS data, the population versus restframe colour is very well fit by the simple sum of two Gaussians. The result is also seen in B04 and strongly suggests two underlying populations of galaxies. This is consistent with the patterns seen in the LFs in B06, where an early type, concentrated, early spectral type, red, high Sérsic index population of galaxies is evident and the LFs binned in absolute magnitude and plotted against their second parameter often show bimodality which is clear even on the log scale used for the axis showing number density.

When the T_{ANN} morphology-density relation is plotted rather than colour-density the distributions are less bimodal, ranging from looking similar to the plots for colour to being not bimodal at all. There are various possible reasons for this, including (1) the morphology may be less sensitive to the processes producing the bimodal population in colour, being intrinsically spread when compared to the colour-producing physics; (2) there may be more than

two populations, the third or more of which the colour may not be sensitive to (an example might be S0 galaxies, which are almost as red as ellipticals); or (3) the neural network morphological types might be spread or biased versus the true types. The last point is not thought to be likely. It is difficult to distinguish between the intrinsic spread or more populations possibilities, although the fact that some of the bins are more bimodal than others favours the third population idea. Here neither possibility is ruled out and indeed both could be occurring. More detailed investigation of the morphology-colour-density relationship may be useful, but it may remain the case that the morphologies are simply intrinsically too ‘fuzzy’ to show the underlying populations as clearly as the colour.

Baldry et al. (2004a) discuss the work in Baldry et al. (2004b) and B04 and agree with the interpretation of morphology, in the sense that ‘whatever processes give rise to the blue/red distribution should also give rise to *distributions* in morphology’, although they go on to say that ‘thus, S0 or Sa galaxies could have a probability of belonging to one or the other distributions and should not be considered as classes’.

The inverse concentration and Sérsic indices show more

Figure 6. As Fig. 5 but for T_{ANN} .Figure 7. Red and early type galaxy fractions in each M_r bin versus Σ_5 for $u - r$ and T_{ANN} . The error bars are 1σ . The left hand panel shows a similar upward trend to fig. 2 of B04.

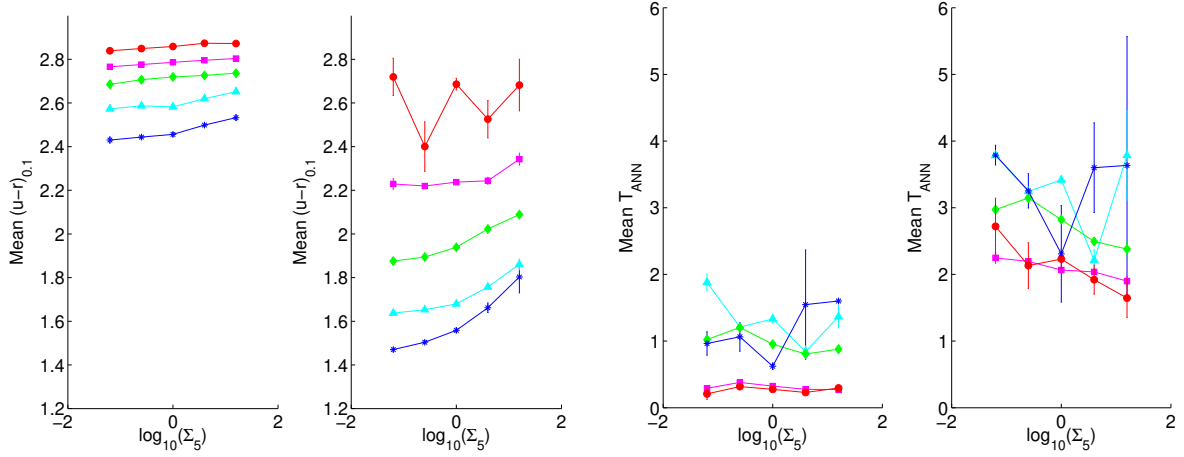


Figure 8. Mean colour and type in each M_r bin versus Σ_5 for red/early and blue/late galaxies, with 1σ error bars. The left hand two plots show $u - r$ and are similar to fig. 3 of B04. The right hand two show T_{ANN} . The magnitude bins are the same as for Fig. 7.

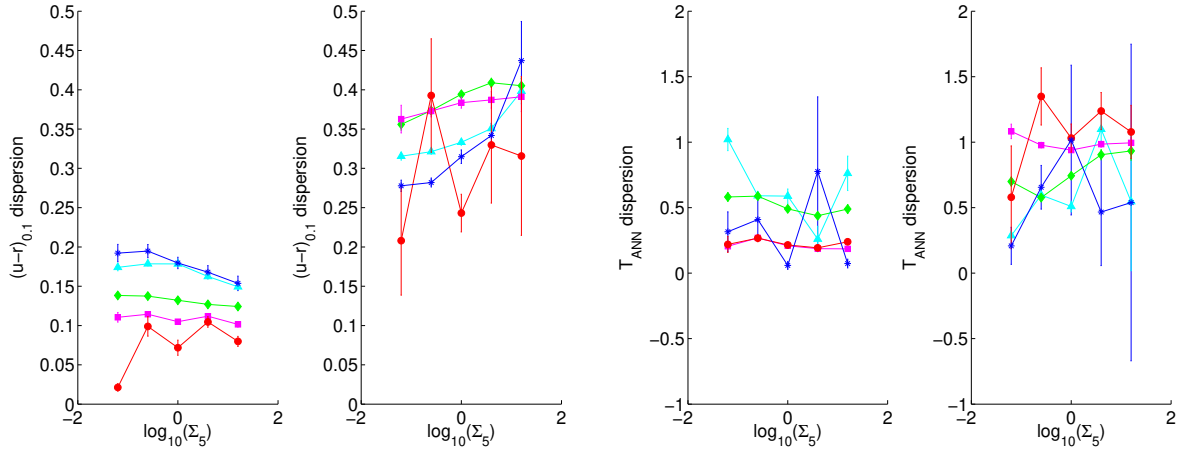


Figure 9. As Fig. 8 but for the σ dispersions in the Gaussian fits.

clearly bimodal distributions, although the CI_{inv} plot becomes unimodal at fainter magnitudes and low densities. As with T_{ANN} , there are no obvious residual relations when those due to colour are removed, thus these measures of morphology are also not predictive of environment beyond their correlation to colour.

The physics giving the bimodal population in colour is thought to be that red galaxies have a passively evolving old stellar population and are formed by major mergers. The blue galaxies are undergoing star formation and less violent accretion events. Galaxies can change from blue to red and when they do they do so rapidly, leaving few galaxies in between the two populations. B04 go on to propose that ‘most star forming galaxies today evolve at a rate that is determined primarily by their intrinsic properties, and independent of environment’, which is consistent with the results here.

The morphology may be seeing extra physics at work, for example ram-pressure stripping of gas from a galaxy infalling into a cluster can turn a spiral into an SO rather than an elliptical, even though they are almost as red. SOs are sufficiently common that they should show up as a component in the plots in this paper if they indeed form one distinct from other galaxies.

At higher redshifts, broad trends include a reduction in the number of S0 galaxies, with a corresponding increase in spirals, and a roughly constant fraction of ellipticals.

For further insight into the physics, comparisons of the observations with the predictions of semi-analytic models would be useful. Until very recently, semi-analytic models have not generally produced bimodal populations, so there may be much to be gained by a detailed intercomparison between the two. One could also compare our results to those at higher redshift.

As well as the measure of the surface density of galaxies here, there are several other measures of environment such as volume density, cluster-centric distance and density or mass of the dark matter halo. The SDSS has various cluster catalogues, described at <http://www.sdss.org/dr4>. The NYU Value-Added Galaxy Catalog also has a density measure. Techniques such as Wiener filtering can use the power spectrum, matter density and bias in a survey to define a density field over a whole volume within the survey. This has been done in the 2dF Galaxy Redshift Survey by Erdo\u0111u et al. (2004) and could also be done for the SDSS.

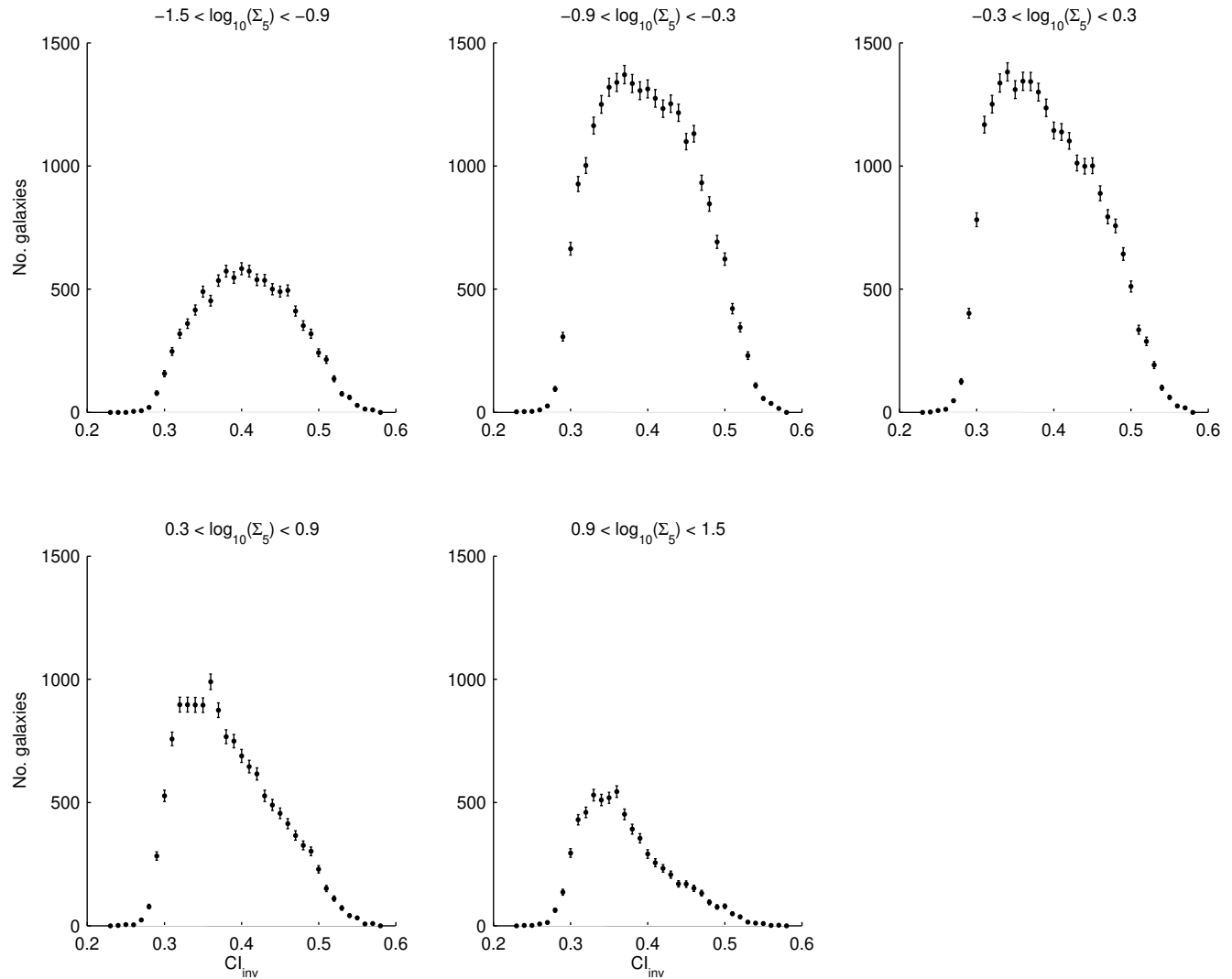


Figure 12. As Fig. 3, but for inverse Petrosian concentration index CI_{inv} . Figs. 12–15 have not been fitted with double Gaussians.

A further parameter that could be incorporated into the framework is the star formation rate, perhaps measured by $EW(H\alpha)$.

Here two Gaussians are fitted. Clearly one could fit more components or different functions, for example if there are three morphological components then three Gaussians may provide a good fit. However, this may still not adequately fit both the excess of intermediate types at $T_{ANN} \sim 1$ and the late types at $T_{ANN} \sim 4$.

The ANN types are biased away from very early or late types, but not to an extent large enough to affect the overall trends seen here. This is thought to be due to the importance of the concentration index in the training set, which has a similar bias. A larger training set for morphology is needed, particularly for very late types.

Here the model $u - r$ colour was used. Driver et al. (2006) showed that the core $u - r$, measured using the PSF colour, provides a cleaner separation for their sample when used in conjunction with the Sérsic index. The same may be true here if that $u - r$ were used, although the model $u - r$ is cleaner than the Petrosian $u - r$, which we also generated results for.

Driver et al. (2006) also argue that the two fundamental com-

ponents are, rather than red and blue galaxies, bulges and discs. This is consistent with the results here.

5 CONCLUSIONS

Galaxy types and properties are studied as a function of environment in the SDSS, specifically the relations between $u - r$ rest-frame colour, Hubble T type assigned by an artificial neural network and Σ_5 surface density of galaxies measured by the fifth nearest neighbour brighter than an r band absolute magnitude of $M_r - 5\log h = -19.5$. The range of density probed covers all environments from the cores of rich clusters to the field.

The colour results are similar to those of Balogh et al. (2004) (B04) but here these are extended to galaxy morphology.

The well-known colour-density and morphology-density relations are seen. The colour is well fit by the sum of two Gaussians, implying two underlying populations, one red and one blue. This was also seen by B04. The mean colour of the red population is approximately constant but the blue population gets slightly redder with increasing density.

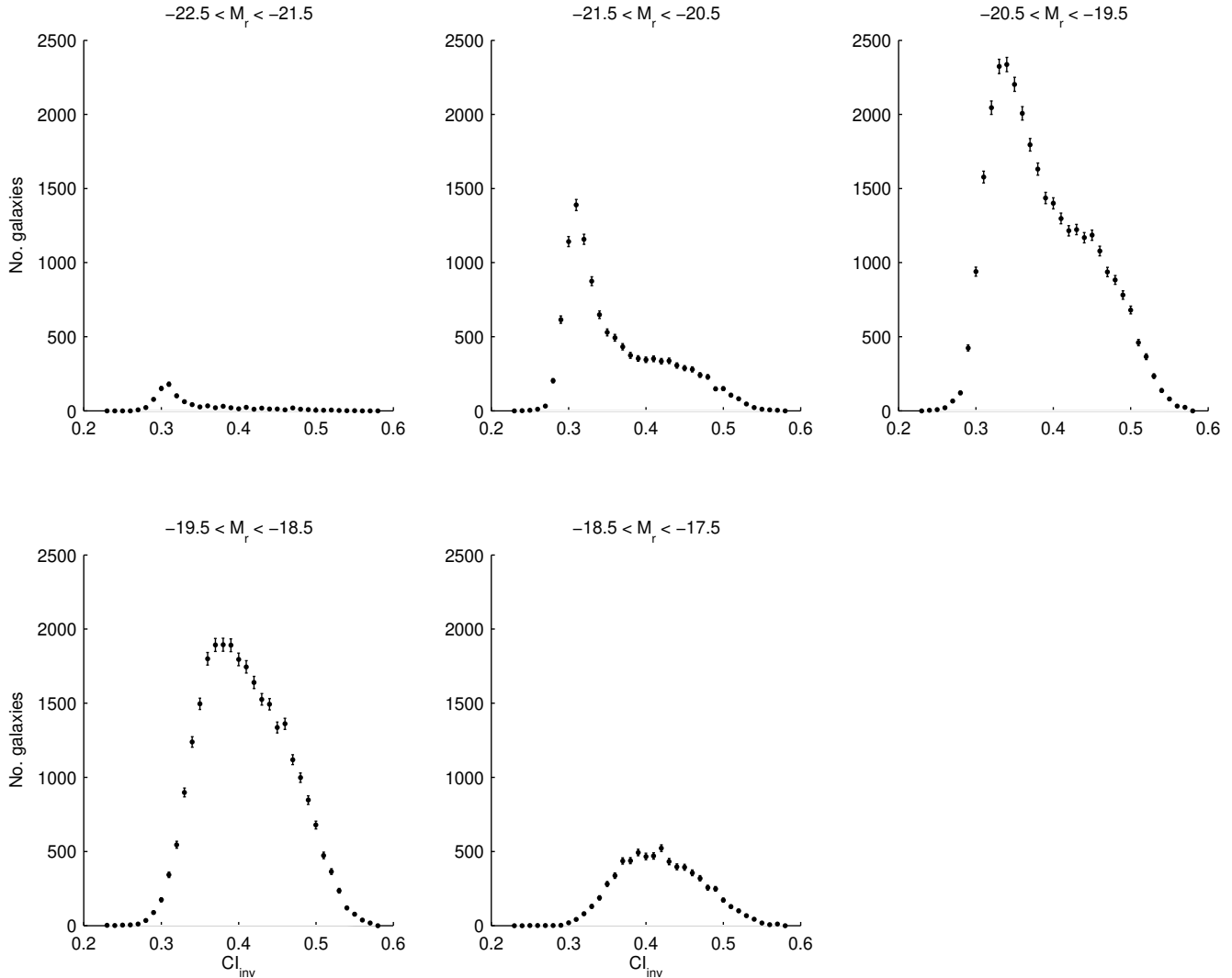


Figure 13. As Fig. 4, but for inverse Petrosian concentration index CI_{inv} .

The morphology-density relation is also seen at high significance over the range of densities probed, thus confirming that the relation extends into the field and is not just present in galaxy clusters. The morphology is less obviously fit by the sum of two Gaussians, suggesting one or more of the possibilities (1) three or more populations (e.g. early, lenticular and late), (2) sensitivity of the morphology to processes which do not affect the colours, or (3) a higher intrinsic spread in morphology compared to two underlying populations and physical processes.

The colour-density relation divided into bins by absolute magnitude reproduces the results of B04: the mean colours are independent of density for fixed luminosity but the red fraction increases with increasing density. The fraction of red galaxies increases approximately linearly with density, with parallel slopes of lower fraction for decreasing luminosity. The dispersion in colour for each population is low for red galaxies, increasing with decreasing luminosity and decreasing with density. For blue galaxies it is significantly higher and shows no significant trend with density.

The morphology-density relation divided in this way is similar if the early type galaxies are red. The early type galaxy fraction increases in a similar way to the fraction of red galaxies but the trend

is noisier. The mean type versus density is similar to colour but the late types do not obviously get earlier with density, consistent with the colour having a stronger dependence on density than morphology. The dispersions show no significant trend with density.

In $u - r$ there is a clear residual relation of galaxies for both blue and red galaxies with density even after the reddening due to the increase in early types is removed. This suggests that colour has a stronger dependence on density than morphology, in agreement with other studies.

For T_{ANN} , there is no evidence of a residual trend once that due to variation with colour is removed.

The inverse concentration and Sérsic indices show more clearly bimodal distributions, although the CI_{inv} plot becomes unimodal at fainter magnitudes and lower densities. Again there are no obvious residual relations when those due to colour are removed, meaning that for the data as presented here, these quantities are also not predictive of environment beyond their correlation to colour.

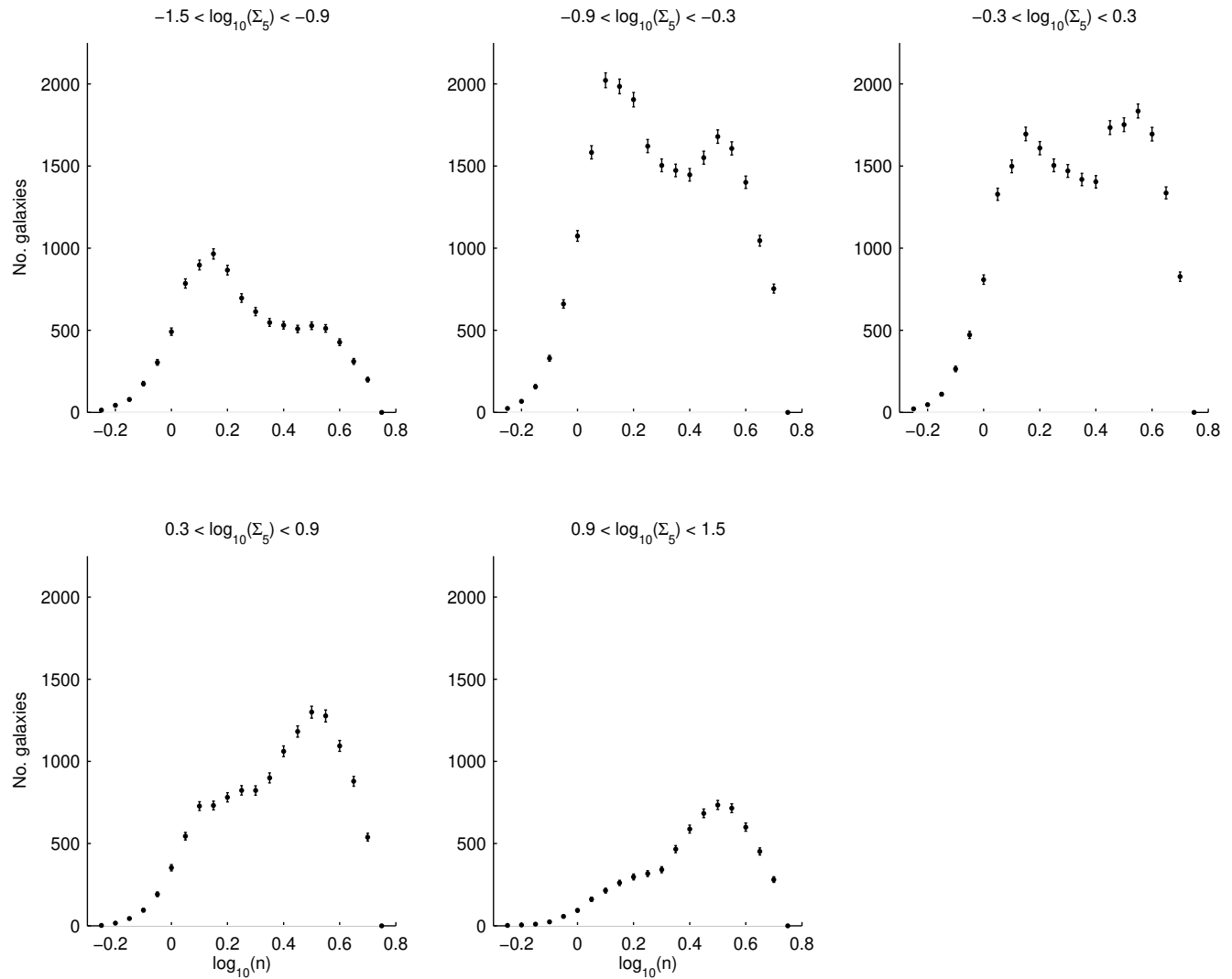


Figure 14. As Fig. 3, but for Sérsic index n .

ACKNOWLEDGMENTS

Nick Ball thanks Bob Nichol, Ivan Baldry, and Michael Balogh for useful discussions, and K. Simon Krughoff and Chris Miller for help with the DR4 VAC catalogue.

Nick Ball was funded by a PPARC studentship. NMB and RJB would like to acknowledge support from NASA through grants NAG5-12578 and NAG5-12580 as well as support through the NSF PACI Project.

Funding for the SDSS and SDSS-II has been provided by the Alfred P. Sloan Foundation, the Participating Institutions, the National Science Foundation, the U.S. Department of Energy, the National Aeronautics and Space Administration, the Japanese Monbukagakusho, the Max Planck Society, and the Higher Education Funding Council for England. The SDSS Web Site is <http://www.sdss.org/>.

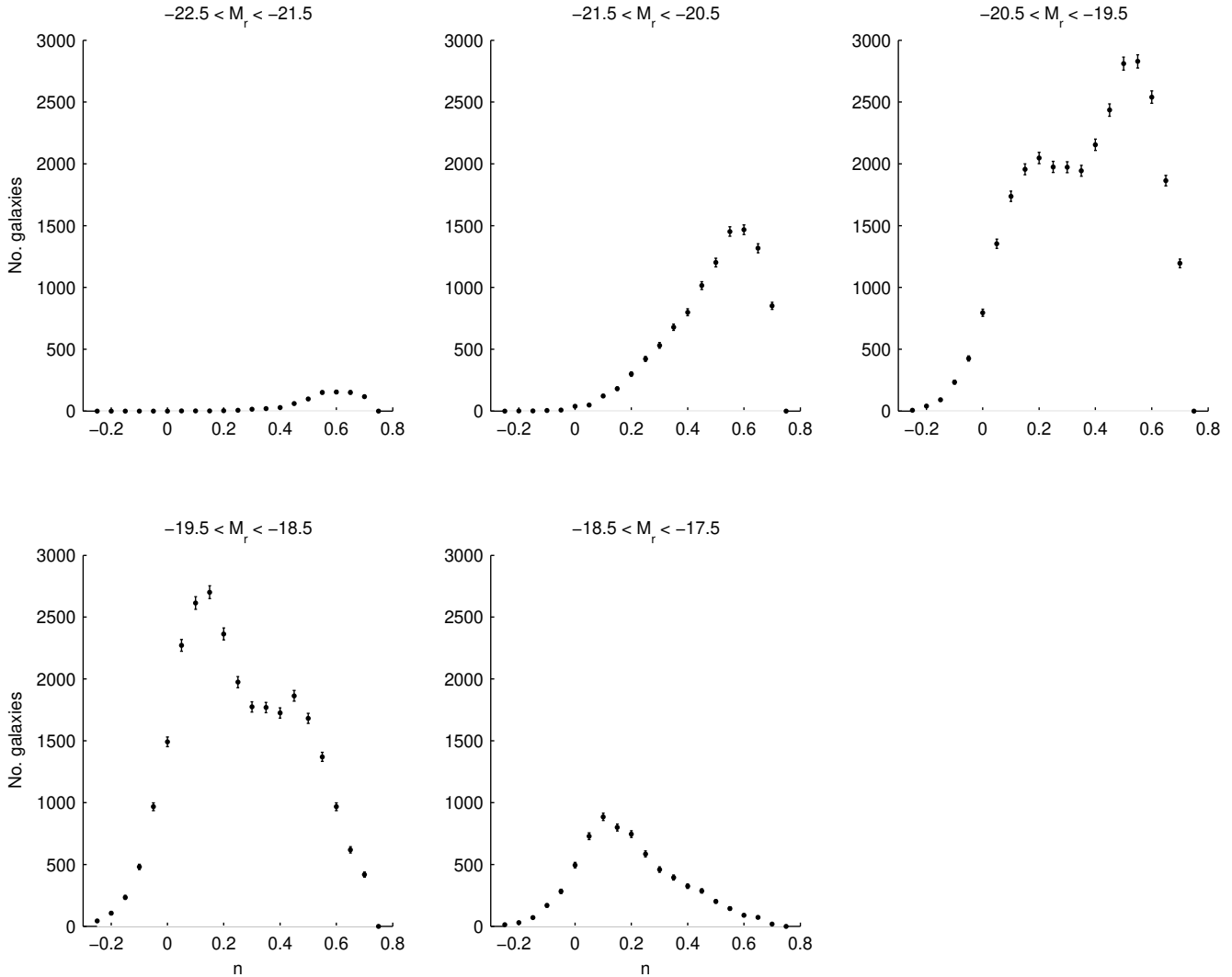
The SDSS is managed by the Astrophysical Research Consortium for the Participating Institutions. The Participating Institutions are the American Museum of Natural History, Astrophysical Institute Potsdam, University of Basel, Cambridge University, Case Western Reserve University, University of Chicago, Drexel

University, Fermilab, the Institute for Advanced Study, the Japan Participation Group, Johns Hopkins University, the Joint Institute for Nuclear Astrophysics, the Kavli Institute for Particle Astrophysics and Cosmology, the Korean Scientist Group, the Chinese Academy of Sciences (LAMOST), Los Alamos National Laboratory, the Max-Planck-Institute for Astronomy (MPA), the Max-Planck-Institute for Astrophysics (MPIA), New Mexico State University, Ohio State University, University of Pittsburgh, University of Portsmouth, Princeton University, the United States Naval Observatory, and the University of Washington.

This research has made use of NASA's Astrophysics Data System.

REFERENCES

- Abbas U., Sheth R. K., 2006, preprint (astro-ph/0601407)
- Adelman-McCarthy J. K. et al., 2006, ApJS, 162, 38
- Avila-Reese V., 2006, preprint (astro-ph/0605212)
- Baldry I. K., Balogh M. L., Bower R., Glazebrook K., Nichol R. C., 2004a, in Allen R. E., Nanopoulos D. V., Pope C. N.,

**Figure 15.** As Fig. 4, but for Sérsic index n .

eds, AIP Conf. Proc. 743: The New Cosmology: Conference on Strings and Cosmology Color bimodality: Implications for galaxy evolution. pp 106–119

Baldry I. K., Glazebrook K., Brinkmann J., Ivezić Ž., Lupton R. H., Nichol R. C., Szalay A. S., 2004b, *ApJ*, 600, 681

Ball N. M., Loveday J., Fukugita M., Nakamura O., Okamura S., Brinkmann J., Brunner R. J., 2004, *MNRAS*, 348, 1038

Ball N. M., Loveday J., Brunner R. J., Baldry I. K., Brinkmann J., 2006, *MNRAS*, in press, preprint (astro-ph/0507547)

Balogh M. L., Baldry I. K., Nichol R., Miller C., Bower R., Glazebrook K., 2004, *ApJL*, 615, L101

Blanton M. R., Lin H., Lupton R. H., Maley F. M., Young N., Zehavi I., Loveday J., 2003, *AJ*, 125, 2276

Blanton M. R. et al., 2005, *AJ*, 129, 2562

Blanton M. R., Eisenstein D., Hogg D. W., Schlegel D. J., Brinkmann J., 2005, *ApJ*, 629, 143

Blanton M. R., Eisenstein D., Hogg D. W., Zehavi I., 2006, *ApJ*, 645, 977

Boselli A., Gavazzi G., 2006, *PASP*, 118, 517

Christlein D., Zabludoff A. I., 2004, *ApJ*, 616, 192

Cooray A., Sheth R., 2002, *PhR*, 372, 1

de Vaucouleurs G., 1948, *Annales d'Astrophysique*, 11, 247

Dressler A., 1980, *ApJ*, 236, 351

Driver S. P. et al., 2006, *MNRAS*, 368, 414

Eisenstein D. J. et al., 2001, *AJ*, 122, 2267

Erdoğdu P. et al., 2004, *MNRAS*, 352, 939

Freeman K. C., 1970, *ApJ*, 160, 811

Fukugita M., Ichikawa T., Gunn J. E., Doi M., Shimasaku K., Schneider D. P., 1996, *AJ*, 111, 1748

Goto T., Yamauchi C., Fujita Y., Okamura S., Sekiguchi M., Smail I., Bernardi M., Gomez P. L., 2003, *MNRAS*, 346, 601

Graham A. W., Driver S. P., 2005, *PASA*, 22, 118

Gunn J. E. et al., 1998, *AJ*, 116, 3040

Gunn J. E. et al., 2006, *AJ*, 131, 2332

Hogg D. W., 2005, preprint (astro-ph/0512029)

Hogg D. W., Finkbeiner D. P., Schlegel D. J., Gunn J. E., 2001, *AJ*, 122, 2129

Ivezić Ž. et al., 2004, *Astronomische Nachrichten*, 325, 583

Lupton R. H., 2006, *AJ*, submitted

Lupton R. H., Gunn J. E., Ivezić Ž., Knapp G. R., Kent S., Yasuda N., 2001, in *ASP Conf. Ser.* 238: *Astronomical Data Analysis Software and Systems X* The SDSS Imaging Pipelines

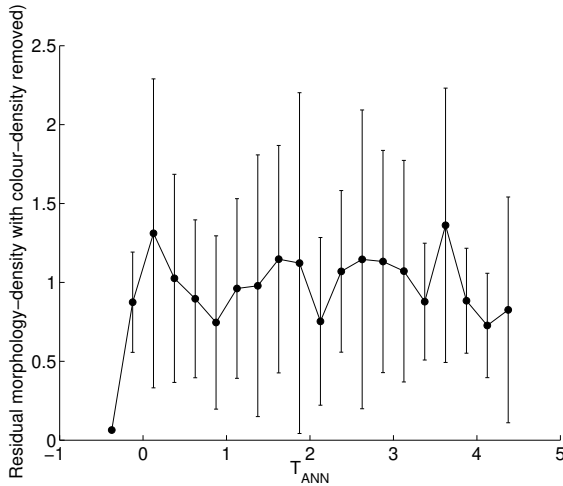


Figure 10. The density dependence of T_{ANN} morphology once the dependence due to $u - r$ colour has been removed. The error bars are the 1σ dispersion in the morphology bins. There is no evidence for a residual relation.

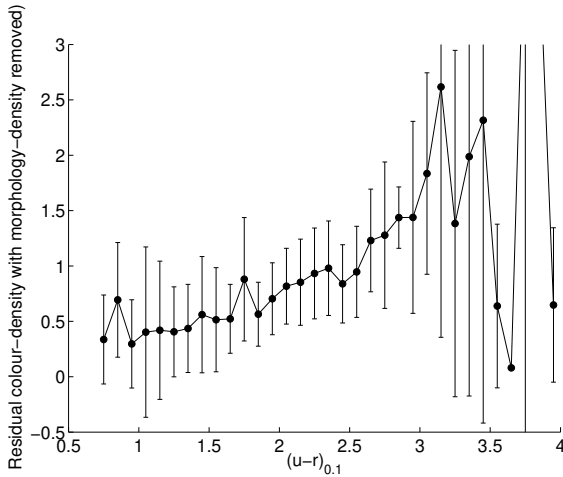


Figure 11. As Fig. 10 but for the residual density dependence of $u - r$ once that due to T_{ANN} has been removed. Unlike morphology, here there is a clear trend.

Naim A., Lahav O., Sodré L., Storrie-Lombardi M. C., 1995, MNRAS, 275, 567
 Pier J. R., Munn J. A., Hindsley R. B., Hennessy G. S., Kent S. M., Lupton R. H., Ivezić Ž., 2003, AJ, 125, 1559
 Richards G. T. et al., 2002, AJ, 123, 2945
 Sérsic J. L., 1968, Atlas de galaxias australes. Cordoba, Argentina: Observatorio Astronomico, 1968
 Smith J. A. et al., 2002, AJ, 123, 2121
 Storrie-Lombardi M. C., Lahav O., Sodré L., Storrie-Lombardi L. J., 1992, MNRAS, 259, 8P
 Stoughton C. et al., 2002, AJ, 123, 485
 Strateva I. et al., 2001, AJ, 122, 1861
 Strauss M. A. et al., 2002, AJ, 124, 1810
 Tucker D. et al., 2006, AN, in press
 Yamauchi C. et al., 2005, AJ, 130, 1545
 York D. G. et al., 2000, AJ, 120, 1579